Supplementary Information

Recycling Plastic Waste for Environmental Remediation in Water Purification and CO_2 Capture

Xinxin Dong[a,b,=], Ammara Akram[a,=], Bibiana Comesaña-Gándara[c], Xinfei Dong[d], Qingchun Ge[d], Ke Wang[a], Shi-Peng Sun[e], Baosheng Jin[b,], Cher Hon Lau[a,*]*

[a]School of Engineering, University of Edinburgh, Robert Stevenson Road, Edinburgh EH9 3FB, UK

[b]Key Laboratory of Energy Thermal Conversion and Control of Ministry of Education, School of Energy & Environment, Southeast University, Nanjing 210096, China

[c]EastChem, School of Chemistry, University of Edinburgh, David Brewster Road, Edinburgh EH9 3FJ, UK

[d]College of Environment and Resources, Fuzhou University, Fujian 350116, China

[e]State Key Laboratory of Materials-Oriented Chemical Engineering, College of Chemical Engineering, Nanjing Tech University, Nanjing 210009, China

[=] These authors contributed equally to this work.

*Corresponding author. E-mail: bsjin@seu.edu.cn, cherhon.lau@ed.ac.uk

CO_2/N_2 selectivity calculations

In the case of binary adsorption, the IAST theory states that the equilibrium relationship between a mixture gas and adsorbed phase should be as the Eqs. (1)- (4), where P_t is the total pressure of mixture gas, y_i and x_i is the molar fraction of gas component in the mixture gas and adsorbent, P_i^0 is the pure adsorbate vapor pressure of component *i* at the spreading pressure (π) of mixture gas. The spreading pressure π for mixture gas has such integral relationship with P_i^0 as Eq. (5), where *A* is the surface area of the adsorbent, *R* is the gas constant (8.314 J mol^{-1} K^{-1}), *T* is the adsorption temperature, Q_i is the adsorption amount of gas component *i*, which is a function of pressure *P*.

$$P_t y_1 = P_1^0 x_1 \tag{1}$$

$$P_t y_2 = P_2^0 x_2 \tag{2}$$

$$y_1 + y_2 = 1 \tag{3}$$

$$x_1 + x_2 = 1 \tag{4}$$

$$\frac{\pi A}{RT} = \int_0^{P_1^0} \frac{Q_1}{P} dp = \int_0^{P_2^0} \frac{Q_2}{P} dp \tag{5}$$

The function between *Q* and *P* could be represented by single site Langmuir-Freundlich (SSLF) model[26], which is displayed in Eq. (6), where *q* is the maximum adsorbed amount of pure gas component at adsorption sites, *b* denotes the affinity parameters for different adsorption sites, *n* is the solid heterogeneity parameter.

$$Q = \frac{qbP^n}{1 + bP^n} \tag{6}$$

At last, the selectivity could be calculated according to the following Eq. (7).

$$S_{1,2} = \frac{x_1 / y_1}{x_2 / y_2} = \frac{P_2^0}{P_1^0} \tag{7}$$

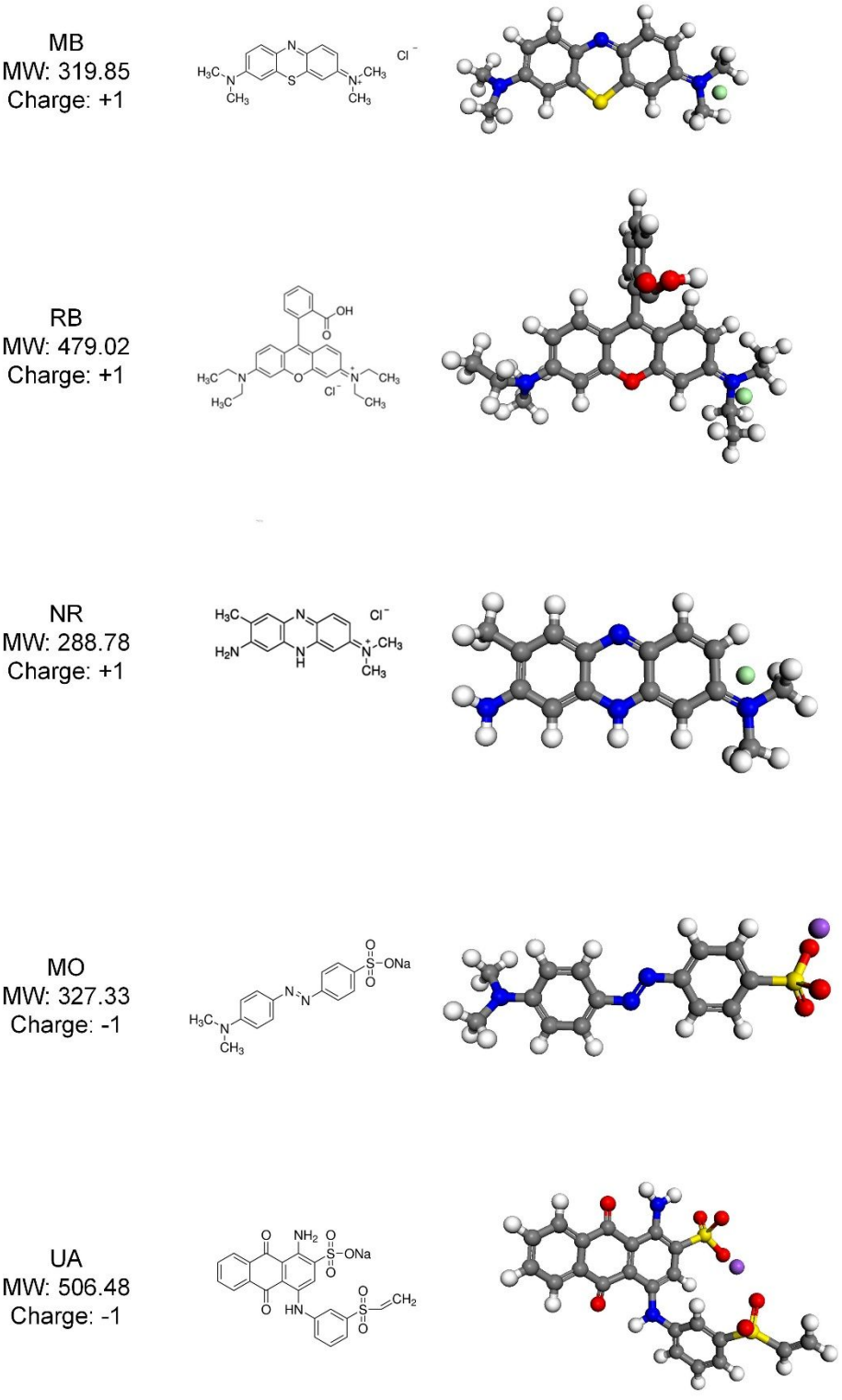

Figure S1. Molecular structure of dyes used in this work.

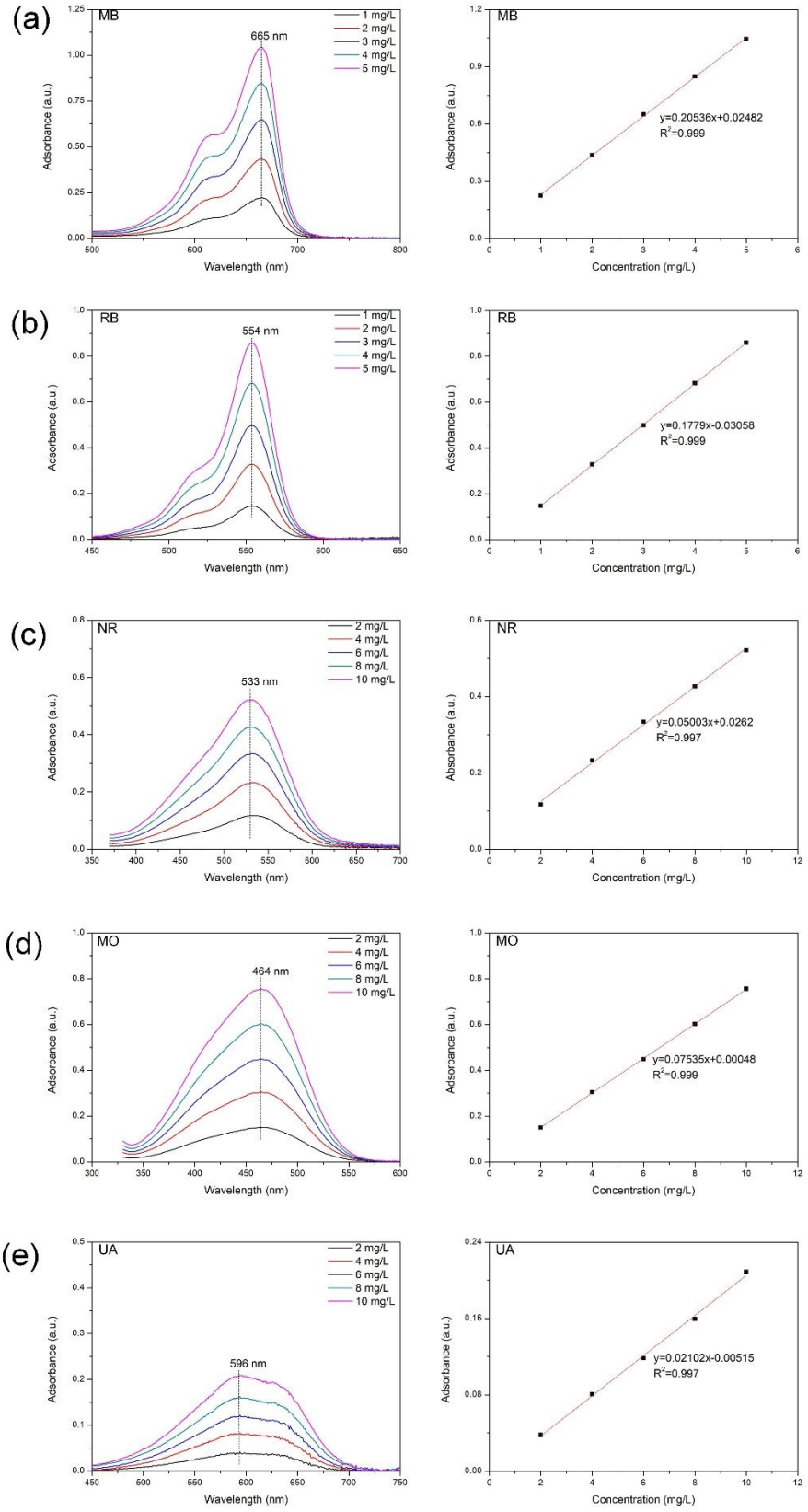

Figure S2. UV-Vis spectra and standard curves of five types of organic dyes: (a) MB, (b) RB, (c) NR, (d) MO and (e) UA.

Dye removal

The adsorption isotherms were fitted using Langmuir and Freundlich isotherm model, which can be mathematically expressed as Eqs. (8)-(10)[27, 28], where C_e (mg/L) is the equilibrium dye concentration, Q_e (mg/g) is the equilibrium adsorption capacity, Q_m (mg/g) is the maximum adsorption capacity, K_L and K_F are the Langmuir and Freundlich constant related to the adsorption capacity, n is the constant representing adsorption intensity, C_0 (mg/L) is the initial dye concentration, V (mL) is the volume of dye solution, m (mg) is the weight of HCP adsorbent.

$$C_e / Q_e = 1/(K_L Q_m) + C_e / Q_m \tag{8}$$

$$\ln Q_e = \ln K_F + 1/n \ln C_e \tag{9}$$

$$Q_e = (C_0 - C_e)V / m \tag{10}$$

Arsenic removal

The pseudo-first order and pseudo-second order kinetics model are utilized to represent the adsorption rate of As(V) on the HCP-3, respectively. Their mathematical expressions are shown in Eqs. (11)-(13), where Q_t (mg/g) is the adsorption capacity at time t (min), Q_e (mg/g) is the equilibrium adsorption capacity, k_1 (min^{-1}) and k_2 ($g \cdot mg^{-1} \cdot min^{-1}$) are the pseudo-first order and pseudo-second order adsorption rate constant, h_0 ($mg \cdot g^{-1} \cdot min^{-1}$) is the pseudo-second order adsorption rate at t=0 min.

$$Q_t = Q_e(1 - e^{-k_1 t}) \tag{11}$$

$$Q_t = \frac{k_2 Q_e^2 t}{1 + k_2 Q_e t} \tag{12}$$

$$h_0 = k_2 Q_e^2 \tag{13}$$

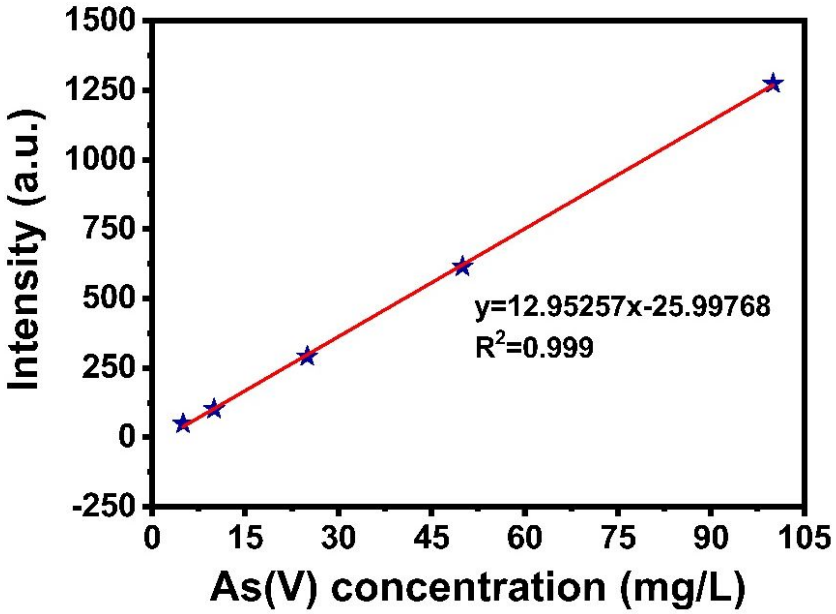

Figure S3. Standard curve of As(V) solution determined from ICP-AES.

Table S1. BET surface area and DFT pore volume of synthesized HCPs.

Type of HCP	BET surface area (m^2/g)	Sequential growth rate (%)	DFT pore volume (cm^3/g)
HCP-1	322	-	0.105
HCP-2	746	132	0.125
HCP-3	1007	35	0.138
HCP-5	1199	19	0.162
HCP-8	252	79	0.082

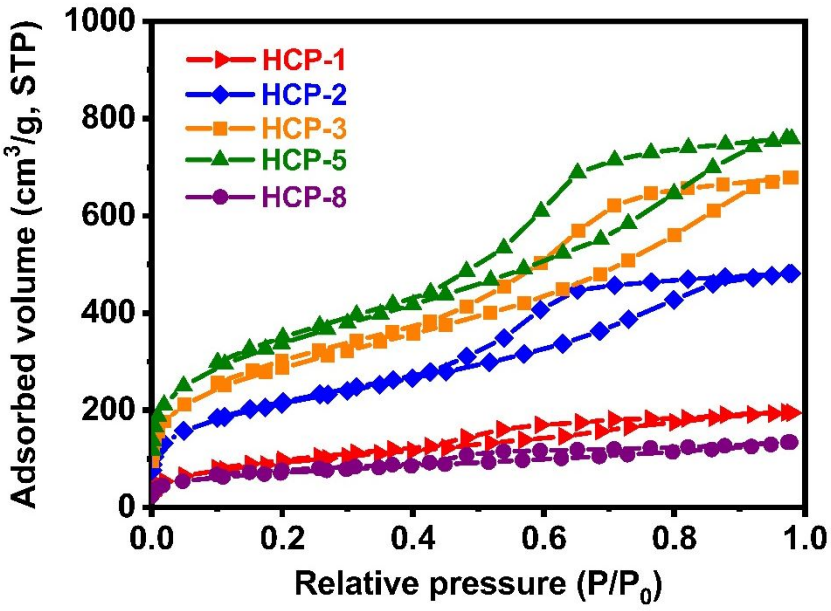

Figure S4. N_2 adsorption isotherms of synthesized HCPs under 77 K.

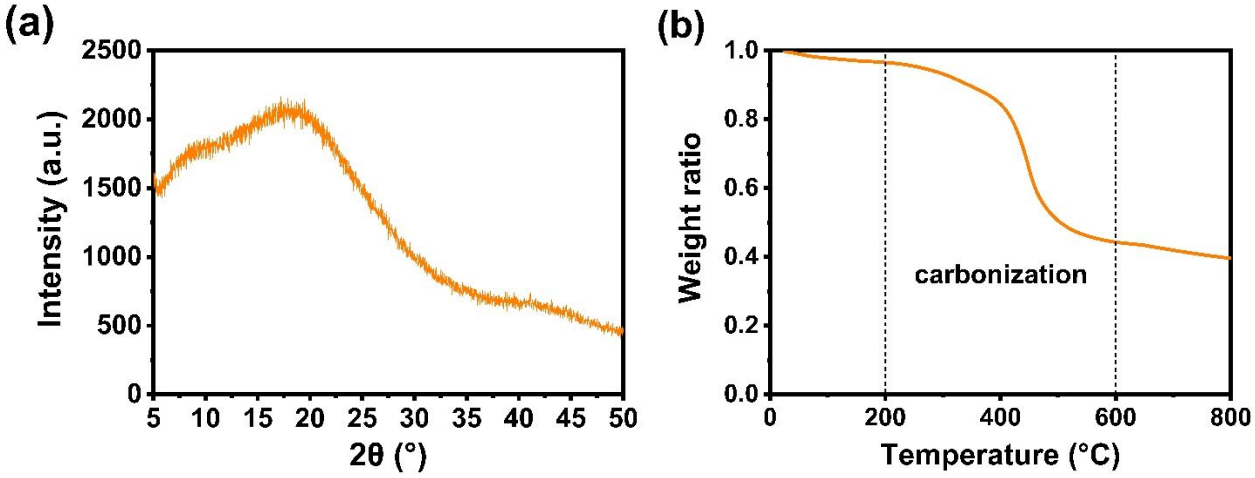

Figure S5. PXRD pattern (a) and TG curve (b) of HCP-3.

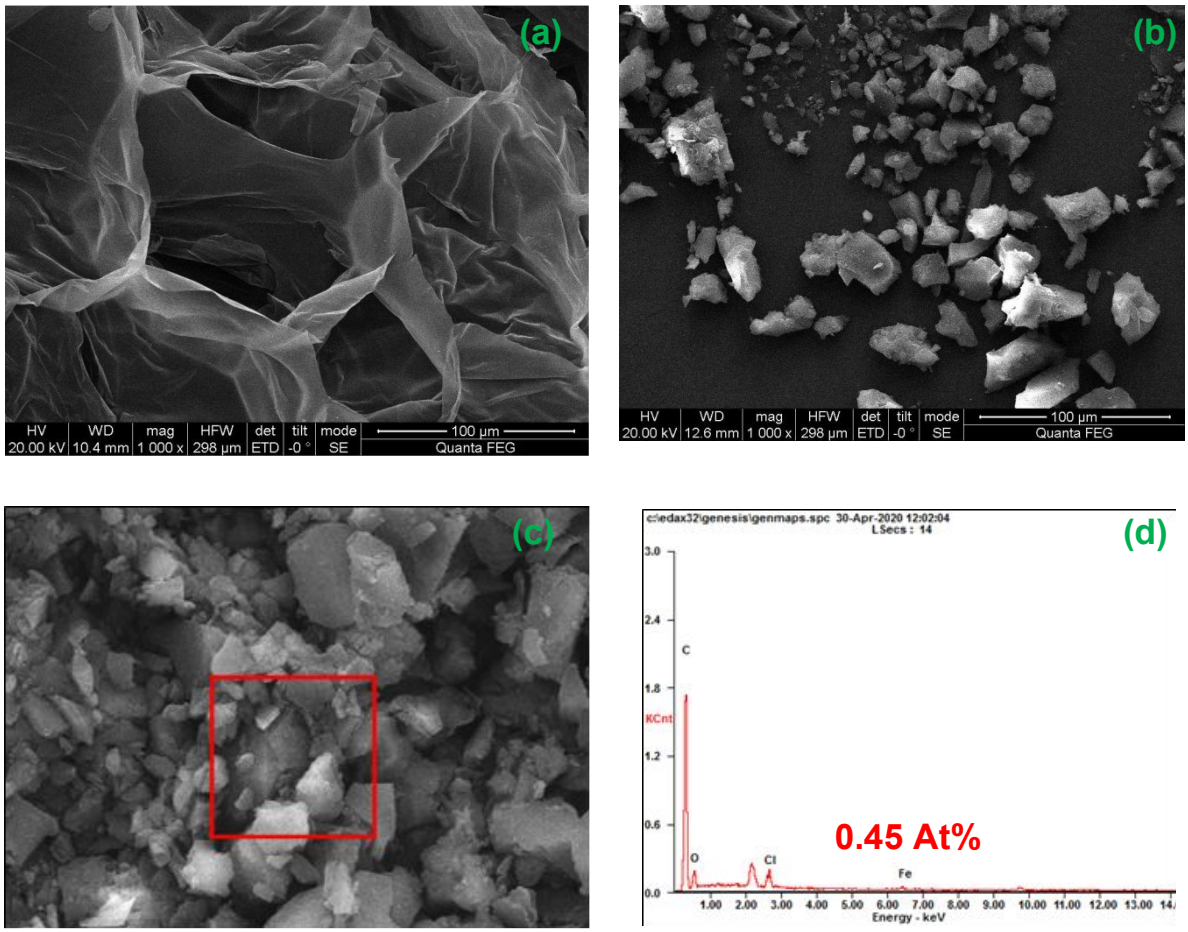

Figure S6. SEM images of WS (a) and HCP-3 (b) plus EDX images (c) and element content (d) of HCP-3.

Table S2. CO_2 and N_2 adsorption capacity at P/P_0=0.99.

Type of HCP	CO_2 uptake (mmol/g)		N_2 uptake (mmol/g)	
	273 K	298 K	273 K	298 K
HCP-1	1.424	0.756	0.102	0.072
HCP-2	1.474	0.832	0.143	0.089
HCP-3	1.728	1.088	0.157	0.093
HCP-5	2.062	1.060	0.147	0.108
HCP-8	0.997	0.577	0.066	0.045

Table S3. SSLF model parameters of CO_2 and N_2 adsorption isotherms.

Type of HCP	Temperature (K)	Adsorbate	*q*	*b*	*n*	R^2
HCP-1	273	CO_2	5.13818	0.00758	1.17598	0.99996
HCP-1	273	N_2	0.42952	0.00324	1.01317	0.99995
HCP-1	298	CO_2	4.28452	0.00282	1.06665	0.99996
HCP-1	298	N_2	8.23817	7.17709E-5	0.96432	0.99913
HCP-2	273	CO_2	5.05706	0.00914	1.21351	0.99995
HCP-2	273	N_2	0.87866	0.00166	0.96804	>0.99999
HCP-2	298	CO_2	3.68544	0.00358	1.04983	0.99996
HCP-2	298	N_2	5.03046	1.58185E-4	0.97308	0.99990
HCP-3	273	CO_2	6.16859	0.00806	1.18943	0.99995
HCP-3	273	N_2	0.94352	0.00176	0.97645	0.99994
HCP-3	298	CO_2	4.70782	0.0043	1.08573	0.99998
HCP-3	298	N_2	0.62628	0.00143	0.96049	0.99997
HCP-5	273	CO_2	7.35625	0.00797	1.18681	0.99982
HCP-5	273	N_2	0.74934	0.00203	0.96126	0.99998
HCP-5	298	CO_2	3.97457	0.00495	1.07272	0.99998
HCP-5	298	N_2	7.41586	1.21269E-4	0.96016	0.99998
HCP-8	273	CO_2	2.32852	0.02160	1.30245	0.99991
HCP-8	273	N_2	0.36557	0.00365	1.12144	0.99860
HCP-8	298	CO_2	2.98763	0.00346	1.09007	0.99996
HCP-8	298	N_2	8.59949	3.41749E-5	0.91628	0.99905

CO_2/N_2 selectivity solving example

The MATLAB code is as the following:

```
function sol=para(a,b,n,c,d,m,Pt,y1,y2)
    function f=fun1(P)
        f=a.*b.*(P.^(n-1))/(1+b.*(P.^n));
    end
    function f=fun2(Q)
        f=c.*d.*(Q.^(m-1))/(1+d.*(Q.^m));
    end
    function h=fun3(X)
        h=integral(@fun1,0,X,'ArrayValued',true)-integral(@fun2,0,X*Pt*y2/(X-Pt*y1),'ArrayValued',true);
    end
sol=fzero(@fun3,[Pt*y1 Pt*y1+10]);
end
```

Results:

```
>> para(6.16859,0.00806,1.18943,0.94352,0.00176,0.97645,50,0.25,0.75)


ans =

   13.0501
```

Verification:

```
>> vpa(int(6.16859*0.00806*x^(1.18943-1)/(1+0.00806*x^1.18943),0,13.0501))

ans =

0.81917388145884510269999584640852

>> vpa(int(0.94352*0.00176*x^(0.97645-1)/(1+0.00176*x^0.97645),0,889.6178))

ans =

0.81913496920589608372101301752496
```

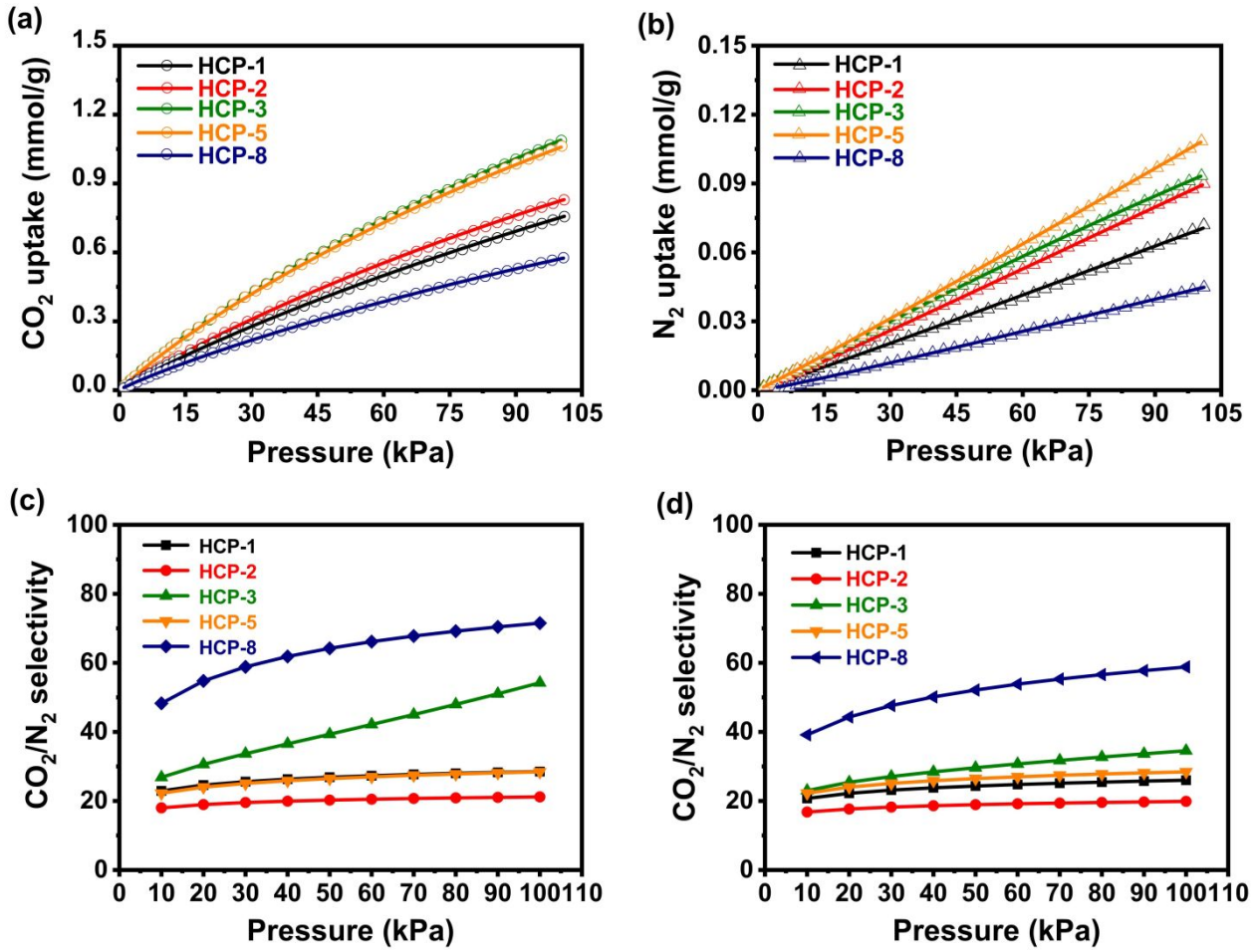

Figure S7. CO_2 and N_2 adsorption isotherms under 298 K and predicted CO_2/N_2 selectivity based on IAST: (a) CO_2 isotherms, (b) N_2 isotherms, (c) CO_2:N_2=1:3 and (d) CO_2:N_2=1:15. The symbols and lines in (a) and (b) represent experimental and SSLF model values, respectively.

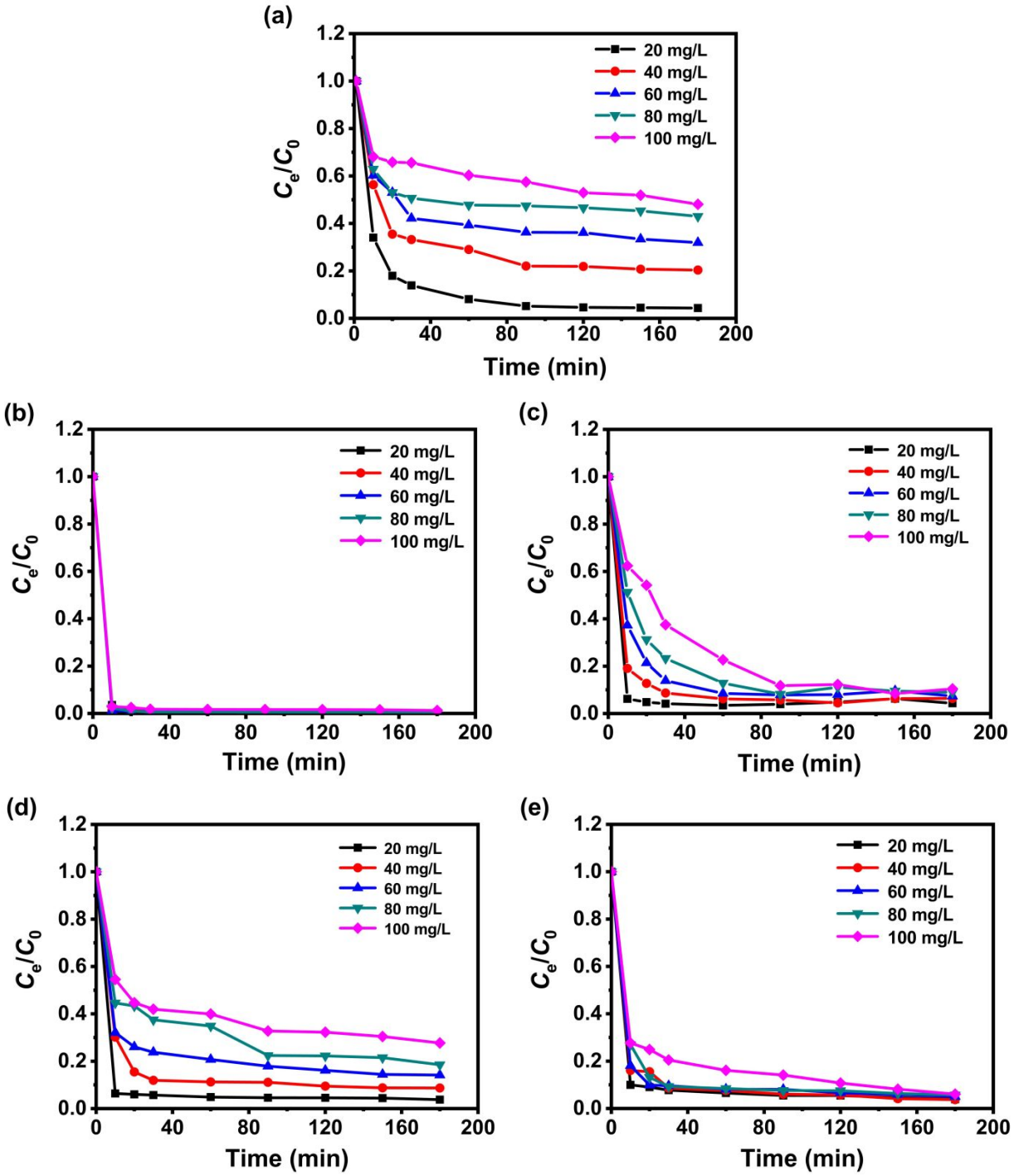

Figure S8. Dye removal performance with time under different concentrations: (a) MB, (b) RB, (c) NR, (d) MO and (e) UA.

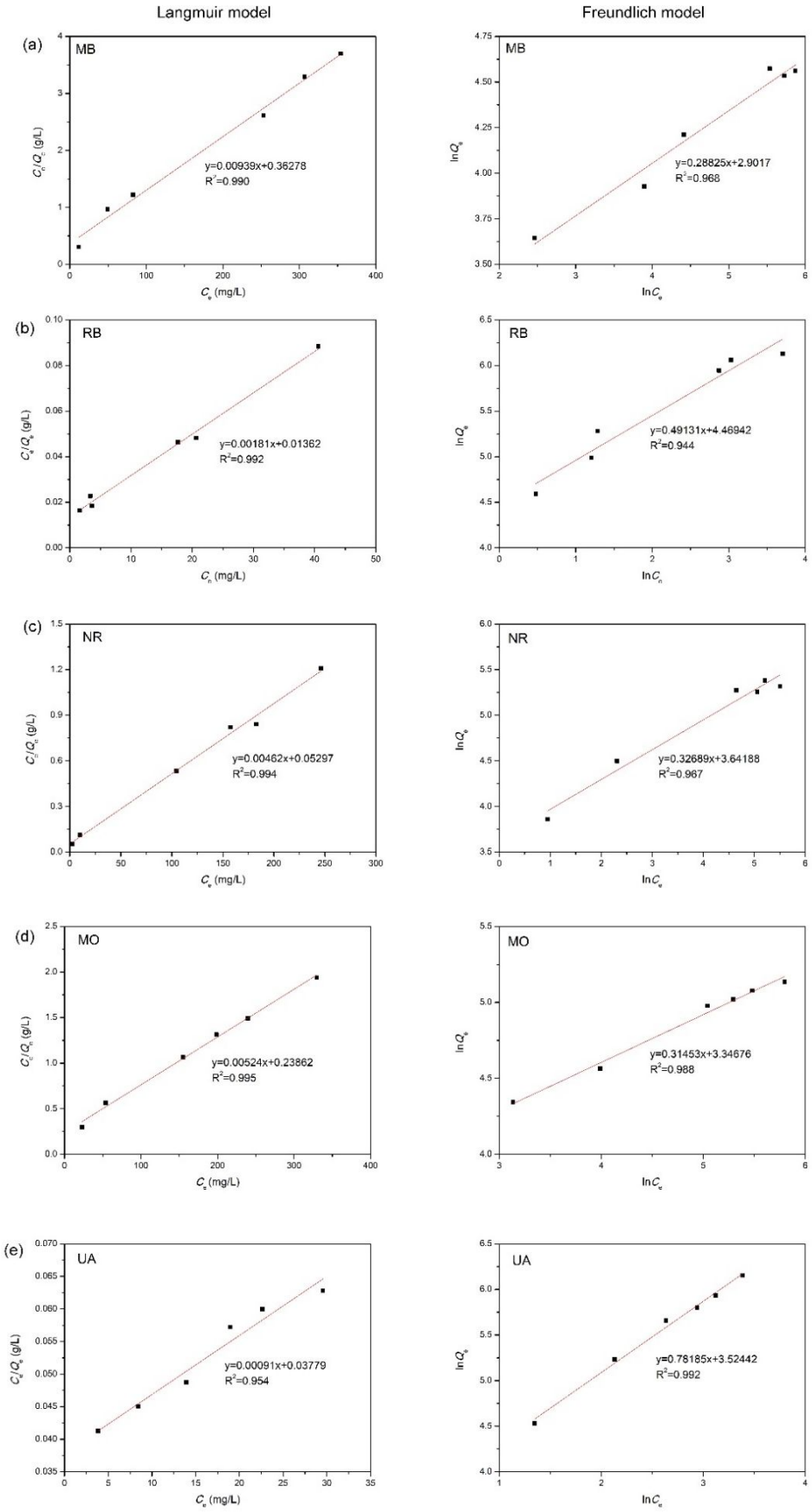

Figure S9. The Langmuir and Freundlich isotherm model fitting: (a) MB, (b) RB, (c) NR, (d)

MO and (e) UA.

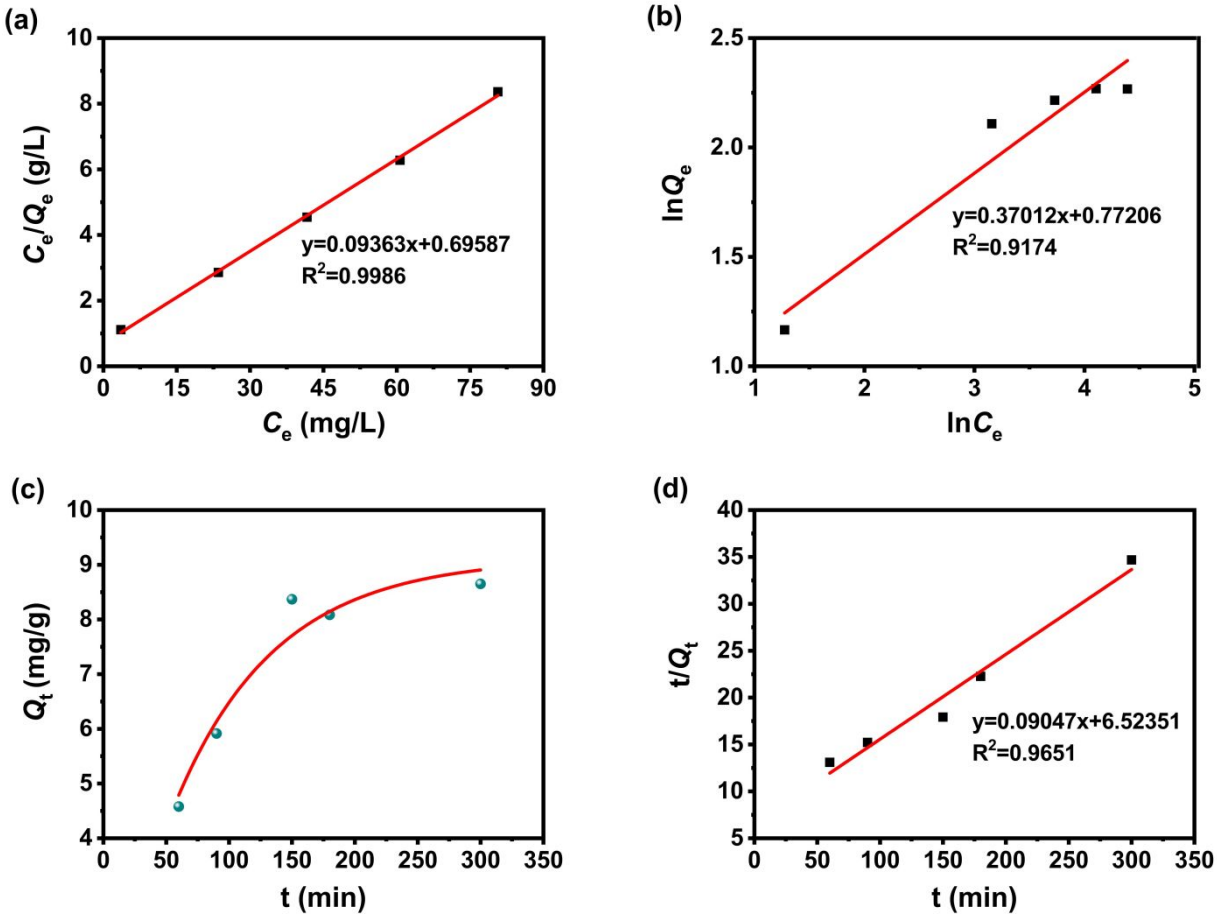

Figure S10. The As(V) isotherm adsorption and kinetic experiment fitting: (a) Langmuir model, (b) Freundlich model, (c) pseudo-first order model and (d) pseudo-second order model.

Table S4. Adsorption kinetics parameters for arsenic uptake.

Pseudo-first order			Pseudo-second order			
k_1	Q_e (mg/g)	R^2	k_2	Q_e (mg/g)	h_0	R^2
0.012	9.13	0.937	1.25E-3	11.05	0.153	0.965

Table S5. Comparison of HCP-3 maximum adsorption capacity of MB with other adsorbents.

Dye	Adsorbent	Adsorbent type	Surface area (m^2/g)	Q_m (mg/g)	Reference
MB	Co22-CuBDC	MOFs	10	52	1
MB	Cu-BTC	MOFs	520	101	2
MB	UiO-66-0.75$(COOH)_2$	MOFs	522	94	3
MB	Cu-Z-GO-M	zeolites	46	94	4
MB	HY	zeolites	631	141	5
MB	ZSM-11	zeolites	432	370	6
MB	ACSO/Fe_3O_4	activated carbon	126	60	7
MB	KGM/AC	activated carbon	352	416	8
MB	AC	activated carbon	285	101	9
MB	AHCP-1	HCPs	939	130	10
MB	**HCP-3**	**HCPs**	**1007**	**106**	**This work**

Table S6. Comparison of HCP-3 maximum adsorption capacity of RB with other adsorbents.

Dye	Adsorbent	Adsorbent type	Surface area (m^2/g)	Q_m (mg/g)	Reference
RB	CoOF	MOFs	199	72	11
RB	NMIL-100(Fe)	MOFs	1	76	12
RB	$MgFe_2O_4$@MOF	MOFs	519	219	13
RB	sodium montmorillonite	zeolites	-	42	14
RB	silicalite-1	zeolites	-	45	15
RB	GB-3	zeolites	249	64	16
RB	STA	activated carbon	670	100	17
RB	CG4	activated carbon	1910	366	18
RB	PAC	activated carbon	471	250	19
RB	SA-MNNPs	HCPs	485	216	20
RB	AHCP-1	HCPs	939	230	10
RB	polyHIPEs/GO	HCPs	-	1.05	21
RB	**HCP-3**	**HCPs**	**1007**	**552.5**	**This work**

Table S7. Comparison of HCP-3 maximum adsorption capacity of NR with other adsorbents.

Dye	Adsorbent	Adsorbent type	Surface area (m^2/g)	Q_m (mg/g)	Reference
NR	$[NH_2(CH_3)_2][In(L)_2]\cdot 2.5DMF\cdot 5H_2O$	MOFs	-	202	22
NR	Si-MCM-41	zeolites	973	288	23
NR	SBA-16	zeolites	742	276	24
NR	BAC	activated carbon	-	171	25
NR	ACF	activated carbon	1556	21	26
NR	OMC-100	activated carbon	993	196	27
NR	AHCP-1	HCPs	939	164	10
NR	**HCP-3**	**HCPs**	**1007**	**216**	**This work**

Table S8. Comparison of HCP-3 maximum adsorption capacity of MO with other adsorbents.

Dye	Adsorbent	Adsorbent type	Surface area (m^2/g)	Q_m (mg/g)	Reference
MO	UiO-66	MOFs	1276	84	28
MO	MFC-N	MOFs	722	130	29
MO	$[Cd(INA)_2(H_2O)].ISB$	MOFs	384	167	30
MO	ILCZ	zeolites	-	38	31
MO	NaA/CuO	zeolites	-	80	32
MO	TNTs@PAC	activated carbon	654	108	19
MO	PEI-STL	activated carbon	2	62	33
MO	MLBCN	activated carbon	82	113	34
MO	HCPANI	HCPs	1083	188	35
MO	HJ-1	HCPs	727	71	36
MO	HAPP	HCPs	104	249	37
MO	**HCP-3**	**HCPs**	**1007**	**191**	**This work**

Table S9. Comparison of HCP-3 As(V) maximum adsorption capacity with other adsorbents.

As type	Adsorbent	Adsorbent type	Surface area (m^2/g)	Q_m (mg/g)	Reference
As(V)	MIL-53(Al)	MOFs	920	15	38
As(V)	MIL-53(Fe)	MOFs	14	21	39
As(V)	Fe-BTC	MOFs	-	12	40
As(V)	WV+NaOH-MZ	zeolites	30	0.02	41
As(V)	FeZr-ZCH	zeolites	339	0.1	42
As(V)	CEZ	zeolites	-	1.5	43
As(V)	GAC-Fe	activated carbon	876	1.4	44
As(V)	Fe-CG	activated carbon	-	3.8	45
As(V)	GACPMF	activated carbon	736	9.5	46
AS(V)	**HCP-3**	**HCPs**	**1007**	**10.7**	**This work**

Table S10. Comparison of HCP-3 IAST CO_2/N_2 selectivity with other adsorbents.

Adsorbent	Adsorbent type	Surface area (m^2/g)	IAST selectivity*	Reference
NJU-Bai50	MOFs	2015	30.5	47
FA_mod-ABA	MOFs	1321	22	48
LIFM-10(Cu)	MOFs	1550	15	49
NaX	zeolites	507	25	50
Co(II)/SSZ-13	zeolites	786	40	51
Zeolite-F	zeolites	54	31	52
SNMC-1-600	activated carbon	1021	37	53
ACDS-800-4	activated carbon	2367	42	54
50CPDA@A-C	activated carbon	1841	25	55
HCP-SC-IMI-SO_3NH_4	HCPs	642	30	56
COP-M-700	HCPs	751	35	57
HCP-3	**HCPs**	**1007**	**43**	**This work**

*calculated based on mixture CO_2/N_2 gas with a composition of 15:85 and pressure of 1 bar at 298 K.

References

(1) Nanthamathee, C. Effect of Co(II) Dopant on The Removal of Methylene Blue by A Dense Copper Terephthalate. *J. Environ. Sci.* **2019,** *81*, 68-79.

(2) Kaur, R.; Kaur, A.; Umar, A.; Anderson, W. A.; Kansal, S. K. Metal Organic Framework (MOF) Porous Octahedral Nanocrystals of Cu-BTC: Synthesis, Properties and Enhanced Adsorption Properties. *Mater. Res. Bull.* **2019,** *109*, 124-133.

(3) Li, T.-T.; Liu, Y.-M.; Wang, T.; Wu, Y.-L.; He, Y.-L.; Yang, R.; Zheng, S.-R. Regulation of The Surface

Area and Surface Charge Property of MOFs by Multivariate Strategy: Synthesis, Characterization, Selective Dye Adsorption and Separation. *Microporous Mesoporous Mater.* **2018,** *272*, 101-108.
(4) Huang, T.; Yan, M.; He, K.; Huang, Z.; Zeng, G.; Chen, A.; Peng, M.; Li, H.; Yuan, L.; Chen, G. Efficient Removal of Methylene Blue from Aqueous Solutions Using Magnetic Graphene Oxide Modified Zeolite. *J. Colloid Interface Sci.* **2019,** *543*, 43-51.
(5) Kasmi, T.; Soualah, A.; Mignard, S.; Batonneau-Gener, I. Effect of Bronsted Acidity of HY Zeolites in Adsorption of Methylene Blue and Comparative Study with Bentonite. *J. Environ. Health Sci. Eng.* **2018,** *16*, 239-247.
(6) Li, H.-J.; Zhou, X.-D.; Di, Y.-H.; Zhang, J.-M.; Zhang, Y. Effect of Si-ATP/CTAB Ratio on Crystal Morphology, Pore Structure and Adsorption Performance of Hierarchical (H) ZSM-11 Zeolite. *Microporous Mesoporous Mater.* **2018,** *271*, 146-155.
(7) Foroutan, R.; Mohammadi, R.; Razeghi, J.; Ramavandi, B. Performance of Algal Activated Carbon/Fe_3O_4 Magnetic Composite for Cationic Dyes Removal from Aqueous Aolutions. *Algal Research* **2019,** *40*, 101509.
(8) Wang, Y.; Li, Y.; Li, H.; Zheng, H.; Du, Q. Equilibrium, Kinetic and Thermodynamic Studies on Methylene Blue Adsorption by Konjac Glucomannan/Activated Carbon Aerogel. *J. Polym. Environ.* **2019,** *27*, 1342-1351.
(9) Yang, B.; Liu, Y.; Liang, Q.; Chen, M.; Ma, L.; Li, L.; Liu, Q.; Tu, W.; Lan, D.; Chen, Y. Evaluation of Activated Carbon Synthesized by One-Stage and Two-Stage Co-Pyrolysis from Sludge and Coconut Shell. *Ecotoxicol Environ. Saf.* **2019,** *170*, 722-731.
(10) Shen, R.; Yan, X.; Guan, Y.-J.; Zhu, W.; Li, T.; Liu, X.-G.; Li, Y.; Gu, Z.-G. One-Pot Synthesis of A Highly Porous Anionic Hypercrosslinked Polymer for Ultrafast Adsorption of Organic Pollutants. *Polym. Chem.* **2018,** *9*, 4724-4732.
(11) Barylak, M.; Cendrowski, K.; Mijowska, E. Application of Carbonized Metal-Organic Framework as Efficient Adsorbent of Cationic Dye. *Ind. Eng. Chem. Res.* **2018,** *57*, 4867-4879.
(12) Duan, S.; Li, J.; Liu, X.; Wang, Y.; Zeng, S.; Shao, D.; Hayat, T. HF-Free Synthesis of Nanoscale Metal-Organic Framework NMIL-100(Fe) as an Efficient Dye Adsorbent. *ACS Sustain. Chem. Eng.* **2016,** *4*, 3368-3378.
(13) Tian, H.; Peng, J.; Lv, T.; Sun, C.; He, H. Preparation and Performance Study of $MgFe_2O_4$/Metal-Organic Framework Composite for Rapid Removal of Organic Dyes from Water. *J. Solid State Chem.* **2018,** *257*, 40-48.
(14) Selvam, P. P.; Preethi, S.; Basakaralingam, P.; Thinakaran, N.; Sivasamy, A.; Sivanesan, S. Removal of Rhodamine B from Aqueous Solution by Adsorption onto Sodium Montmorillonite. *J. Hazard. Mater.* **2008,** *155*, 39-44.
(15) Sabarish, R.; Unnikrishnan, G. Novel Biopolymer Templated Hierarchical Silicalite-1 as An Adsorbent for The Removal of Rhodamine B. *J. Mol. Liq.* **2018,** *272*, 919-929.
(16) Cheng, Z.-L.; Li, Y.-X.; Liu, Z. Novel Adsorption Materials Based on Graphene Oxide/Beta Zeolite Composite Materials and Their Adsorption Performance for Rhodamine B. *J. Alloys Compd.* **2017,** *708*,

255-263.
(17) Jedynak, K.; Wideł, D.; Rędzia, N. Removal of Rhodamine B (A Basic Dye) and Acid Yellow 17 (An Acidic Dye) from Aqueous Solutions by Ordered Mesoporous Carbon and Commercial Activated Carbon. *Colloids Interfaces* **2019,** *3*, 30.
(18) Wen, X.; Liu, H.; Zhang, L.; Zhang, J.; Fu, C.; Shi, X.; Chen, X.; Mijowska, E.; Chen, M. J.; Wang, D. Y. Large-Scale Converting Waste Coffee Grounds into Functional Carbon Materials as High-Efficient Adsorbent for Organic Dyes. *Bioresour. Technol.* **2019,** *272*, 92-98.
(19) Lin, Y.; Ma, J.; Liu, W.; Li, Z.; He, K. Efficient Removal of Dyes from Dyeing Wastewater by Powder Activated Charcoal/Titanate Nanotube Nanocomposites: Adsorption and Photoregeneration. *Environ. Sci. Pollut. Res. Int.* **2019,** *26*, 10263-10273.
(20) Li, Q.; Zhan, Z.; Jin, S.; Tan, B. Wettable Magnetic Hypercrosslinked Microporous Nanoparticle as An Efficient Adsorbent for Water Treatment. *Chem. Eng. J.* **2017,** *326*, 109-116.
(21) Huang, Y.; Ruan, G.; Ruan, Y.; Zhang, W.; Li, X.; Du, F.; Hu, C.; Li, J. Hypercrosslinked Porous Polymers Hybridized with Graphene Oxide for Water Treatment: Dye Adsorption and Degradation. *RSC Adv.* **2018,** *8*, 13417-13422.
(22) Zhang, B.; Chu, Q. Q.; Yue, K. F.; Zhang, S. H.; Liu, B.; Wang, Y. Y. A Flexible and Stable Interpenetrated Indium Pyridylcarboxylate Framework with Breathing Behaviors and Highly Selective Adsorption of Cationic Dyes. *Inorg. Chem.* **2019,** *58*, 4019-4025.
(23) Chaudhuri, H.; Dash, S.; Sarkar, A. Adsorption of Different Dyes from Aqueous Solution Using Si-MCM-41 Having Very High Surface Area. *J. Porous Mater.* **2016,** *23*, 1227-1237.
(24) Chaudhuri, H.; Dash, S.; Ghorai, S.; Pal, S.; Sarkar, A. SBA-16: Application for The Removal of Neutral, Cationic, and Anionic Dyes from Aqueous Medium. *J. Environ. Chem. Eng.* **2016,** *4*, 157-166.
(25) Luo, H.; Zhang, S.; Li, X.; Xu, Q.; Liu, J.; Wang, Z. A facile Route for Preparation of Magnetic Biomass Activated Carbon with High Performance for Removal of Dye Pollutants. *Environ. Sci. Pollut. Res. Int.* **2017,** *24*, 15599-15608.
(26) Zhang, L.; Tu, L.-y.; Liang, Y.; Chen, Q.; Li, Z.-s.; Li, C.-h.; Wang, Z.-h.; Li, W. Coconut-Based Activated Carbon Fibers for Efficient Adsorption of Various Organic Dyes. *RSC Adv.* **2018,** *8*, 42280-42291.
(27) Yuan, X.; Zhuo, S. P.; Xing, W.; Cui, H. Y.; Dai, X. D.; Liu, X. M.; Yan, Z. F. Aqueous Dye Adsorption on Ordered Mesoporous Carbons. *J. Colloid Interface Sci.* **2007,** *310*, 83-89.
(28) Molavi, H.; Hakimian, A.; Shojaei, A.; Raeiszadeh, M. Selective Dye Adsorption by Highly Water Stable Metal-Organic Framework: Long Term Stability Analysis in Aqueous Media. *Appl. Surf. Sci.* **2018,** *445*, 424-436.
(29) Huang, L.; He, M.; Chen, B.; Hu, B. Magnetic Zr-MOFs Nanocomposites for Rapid Removal of Heavy Metal Ions and Dyes from Water. *Chemosphere* **2018,** *199*, 435-444.
(30) Tella, A. C.; Olawale, M. D.; Neuburger, M.; Obaleye, J. A. Synthesis and Crystal Structure of Cd-Based Metal-Organic Framework for Removal of Methyl-Orange from Aqueous Solution. *J. Solid State Chem.* **2017,** *255*, 157-166.
(31) Xing, X.; Chang, P.-H.; Lv, G.; Jiang, W.-T.; Jean, J.-S.; Liao, L.; Li, Z. Ionic-Liquid-Crafted Zeolite for

The Removal of Anionic Dye Methyl Orange. *J. Taiwan Inst. Chem. Eng.* **2016,** *59*, 237-243.
(32) Mekatel, E. H.; Amokrane, S.; Aid, A.; Nibou, D.; Trari, M. Adsorption of Methyl Orange on Nanoparticles of A Synthetic Zeolite NaA/CuO. *C.R. Chim.* **2015,** *18*, 336-344.
(33) Wong, S.; Tumari, H. H.; Ngadi, N.; Mohamed, N. B.; Hassan, O.; Mat, R.; Saidina Amin, N. A., Adsorption of Anionic Dyes on Spent Tea Leaves Modified with Polyethyleneimine (PEI-STL). *J. Cleaner Prod.* **2019,** *206*, 394-406.
(34) Ma, Y.-z.; Zheng, D.-f.; Mo, Z.-y.; Dong, R.-j.; Qiu, X.-q. Magnetic Lignin-Based Carbon Nanoparticles and The Adsorption for Removal of Methyl Orange. *Colloids Surf. A* **2018,** *559*, 226-234.
(35) Sharma, V.; Rekha, P.; Mohanty, P. Nanoporous Hypercrosslinked Polyaniline: An Efficient Adsorbent for The Adsorptive Removal of Cationic and Anionic Dyes. *J. Mol. Liq.* **2016,** *222*, 1091-1100.
(36) Huang, J.-H.; Huang, K.-L.; Liu, S.-Q.; Wang, A. T.; Yan, C. Adsorption of Rhodamine B and Methyl Orange on A Hypercrosslinked Polymeric Adsorbent in Aqueous Solution. *Colloids Surf. A* **2008,** *330*, 55-61.
(37) He, Y.; Li, H.; Zhou, L.; Xu, T.; Peng, C.; Liu, H. Removal of Methyl Orange from Aqueous Solutions by A Novel Hyper-Cross-Linked Aromatic Triazine Porous Polymer. *Acta Phys. Chim. Sin.* **2019,** *35*, 299-306.
(38) Li, J.; Wu, Y. N.; Li, Z.; Zhu, M.; Li, F. Characteristics of Arsenate Removal from Water by Metal-Organic Frameworks (MOFs). *Water Sci. Technol.* **2014,** *70*, 1391-1397.
(39) Vu, T. A.; Le, G. H.; Dao, C. D.; Dang, L. Q.; Nguyen, K. T.; Nguyen, Q. K.; Dang, P. T.; Tran, H. T. K.; Duong, Q. T.; Nguyen, T. V.; Lee, G. D. Arsenic Removal from Aqueous Solutions by Adsorption Using Novel MIL-53(Fe) as A Highly Efficient Adsorbent. *RSC Adv.* **2015,** *5*, 5261-5268.
(40) Zhu, B.-J.; Yu, X.-Y.; Jia, Y.; Peng, F.-M.; Sun, B.; Zhang, M.-Y.; Luo, T.; Liu, J.-H.; Huang, X.-J. Iron and 1,3,5-Benzenetricarboxylic Metal-Organic Coordination Polymers Prepared by Solvothermal Method and Their Application in Efficient As(V) Removal from Aqueous Solutions. *J. Phys. Chem. C* **2012,** *116*, 8601-8607.
(41) Liu, Z. W.; Cao, C. X.; Han, B. H. A Cationic Porous Organic Polymer for High-Capacity, Fast, and Selective Capture of Anionic Pollutants. *J. Hazard. Mater.* **2019,** *367*, 348-355.
(42) Velazquez-Peña, G. C.; Solache-Ríos, M.; Olguin, M. T.; Fall, C. As(V) Sorption by Different Natural Zeolite Frameworks Modified with Fe, Zr and FeZr. *Microporous Mesoporous Mater.* **2019,** *273*, 133-141.
(43) Pillewan, P.; Mukherjee, S.; Kumar Meher, A.; Rayalu, S.; Bansiwal, A. Removal of Arsenic (III) and Arsenic (V) Using Copper Exchange Zeolite-A. *Environ. Prog. Sustainable Energy* **2014**, *33*, 1274-1282.
(44) Kalaruban, M.; Loganathan, P.; Nguyen, T. V.; Nur, T.; Hasan Johir, M. A.; Nguyen, T. H.; Trinh, M. V.; Vigneswaran, S. Iron-Impregnated Granular Activated Carbon for Arsenic Removal: Application to Practical Column Filters. *J. Environ. Manage.* **2019,** *239*, 235-243.
(45) Pintor, A. M. A.; Vieira, B. R. C.; Santos, S. C. R.; Boaventura, R. A. R.; Botelho, C. M. S. Arsenate and Arsenite Adsorption onto Iron-Coated Cork Granulates. *Sci. Total Environ.* **2018,** *642*, 1075-1089.
(46) Roh, J. S.; Park, J.-S.; Roh, J. M.; Park, H. B.; Do, S.-H. The Pretreatment of Granular Activated Carbon Using Sodium Persulfate and Hydrogen Peroxide under Basic Conditions: Properties, Metal

Impregnation, and As(V) Adsorption. *Mater. Chem. Phys.* **2018,** *218*, 317-325.
(47) Song, X.; Zhang, M.; Duan, J.; Bai, J. Constructing and Finely Tuning the CO_2 Traps of Stable and Various-Pore-Containing MOFs towards Highly Selective CO_2 Capture. *Chem. Commun.* **2019,** *55*, 3477-3480.
(48) Koutsianos, A.; Kazimierska, E.; Barron, A. R.; Taddei, M.; Andreoli, E. A New Approach to Enhancing The CO_2 Capture Performance of Defective UiO-66 via Post-Synthetic Defect Exchange. *Dalton Trans.* **2019,** *48*, 3349-3359.
(49) Xiong, Y.; Fan, Y. Z.; Yang, R.; Chen, S.; Pan, M.; Jiang, J. J.; Su, C. Y. Amide and N-Oxide Functionalization of T-Shaped Ligands for Isoreticular MOFs with Giant Enhancements in CO_2 Separation. *Chem. Commun.* **2014,** *50*, 14631-14634.
(50) Salehi, S.; Anbia, M. Characterization of CPs/Ca-Exchanged FAU- and LTA-Type Zeolite Nanocomposites and Their Selectivity for CO_2 and N_2 Adsorption. *J. Phys. Chem. Solids* **2017,** *110*, 116-128.
(51) Sun, M.; Gu, Q.; Hanif, A.; Wang, T.; Shang, J. Transition Metal Cation-Exchanged SSZ-13 Zeolites for CO_2 Capture and Separation from N_2. *Chem. Eng. J.* **2019,** *370*, 1450-1458.
(52) Belani, M. R.; Somani, R. S.; Bajaj, H. C. Sorption of Carbon Dioxide, Methane, and Nitrogen on Zeolite-F: Equilibrium Adsorption Study. *Environ. Prog. Sustainable Energy* **2017,** *36*, 850-856.
(53) Zhang, P.; Zhong, Y.; Ding, J.; Wang, J.; Xu, M.; Deng, Q.; Zeng, Z.; Deng, S. A New Choice of Polymer Precursor for Solvent-Free Method: Preparation of N-Enriched Porous Carbons for Highly Selective CO_2 Capture. *Chem. Eng. J.* **2019,** *355*, 963-973.
(54) Li, J.; Michalkiewicz, B.; Min, J.; Ma, C.; Chen, X.; Gong, J.; Mijowska, E.; Tang, T. Selective Preparation of Biomass-Derived Porous Carbon with Controllable Pore Sizes toward Highly Efficient CO_2 Capture. *Chem. Eng. J.* **2019,** *360*, 250-259.
(55) Liang, W.; Liu, Z.; Peng, J.; Zhou, X.; Wang, X.; Li, Z. Enhanced CO_2 Adsorption and $CO_2/N_2/CH_4$ Selectivity of Novel Carbon Composites CPDA@A-Cs. *Energy Fuels* **2018,** *33*, 493-502.
(56) Alahmed, A. H.; Briggs, M. E.; Cooper, A. I.; Adams, D. J. Covalent and Electrostatic Incorporation of Amines into Hypercrosslinked Polymers for Increased CO_2 Selectivity. *J. Polym. Sci. A* **2018,** *56*, 2513-2521.
(57) Modak, A.; Bhaumik, A. Porous Carbon Derived via KOH Activation of A Hypercrosslinked Porous Organic Polymer for Efficient CO_2, CH_4, H_2 adsorptions and high CO_2/N_2 Selectivity. *J. Solid State Chem.* **2015,** *232*, 157-162.